AN ANALYTICAL METHOD FOR PREDICTING THE STABILITY AND CONTROL CHARACTERISTICS OF LARGE ELASTIC AIRPLANES AT SUBSONIC AND SUPERSONIC SPEEDS

PART II: APPLICATION

By

Howard L. Chevalier
Research Scientist
Ames Research Center, National Aeronautics and Space Administration
Moffett Field, California, U.S.A. 94035

Gerald M. Dornfeld and Robert C. Schwanz
Research Engineers
Aerodynamics Research Staff, Commercial Airplane Division
The Boeing Company, Renton, Washington, U.S.A.

SUMMARY

The method is applied to two aircraft representative of current design, the Boeing 707-320B and an early version of the supersonic transport. Comparisons with experimental values indicate that this purely analytical method provides reliable and useful results for estimating the longitudinal stability and control characteristics of large flexible aircraft. The effects of elasticity on the static longitudinal stability and control of the two aircraft were found to be large and unfavorable for most flight conditions. On the other hand, elasticity did not greatly affect the dynamic stability characteristics, but the results indicate that as the structural frequencies approach the frequency of motion of the airplane (ratios less than 4:1), major effects might occur.

INTRODUCTION

It is evident (1) that the analytical determination of the stability and control of an elastic airplane involves three basic considerations: (i) prediction of the aerodynamic forces, (ii) determination of the deformations in shape caused by these forces and the ensuing effects upon the forces themselves, and (iii) combination of these results to determine the dynamic motion of the airplane and its structure. Errors in the analytical results will accrue from all of these sources.

Experience has shown that the aerodynamic problem is the most difficult to treat, and the aerodynamic predictions contain large uncertainties. For these reasons an assessment of the utility of an analytic scheme for computing stability characteristics should include the validity of the aerodynamic analysis in addition to the overall accuracy of the scheme itself. Such an appraisal has already been made of the aerodynamic method of the present scheme, but is concerns only idealized wing-body shapes (2,3). The presence of nacelles, struts, hinge lines, and various other protuberances and surface discontinuities on airplanes, together with the large differences between wind tunnel and flight Reynolds number, makes it advisable to extend the appraisal to full-scale aircraft. This extension is the first objective of the present investigation.

A second, more important objective, is to determine the overall accuracy of the analytical scheme applied to elastic aircraft, thereby assessing its general usefulness in aircraft design.

To accomplish these two objectives, information concerning the effects of elasticity on the stability and control of the associated configurations is supplemented and re-examined to determine how and to what extent the principal stability and control parameters of the configurations are affected.

With but one exception all results apply only to longitudinal motion.

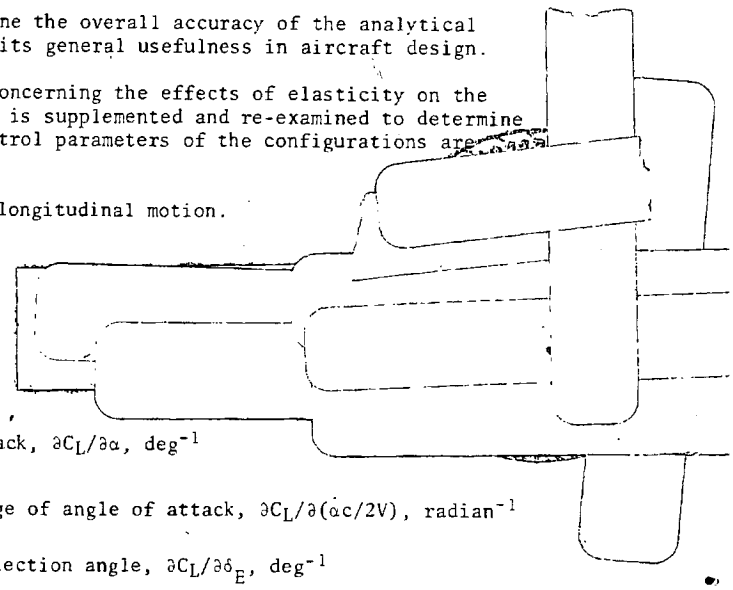

SYMBOLS

b	wing span, m
C_L	lift coefficient, $L/q_\infty S$
C_{L_α}	change in lift coefficient with angle of attack, $\partial C_L/\partial\alpha$, deg^{-1}
$C_{L_{\dot\alpha}}$	change in lift coefficient with rate of change of angle of attack, $\partial C_L/\partial(\dot\alpha c/2V)$, $radian^{-1}$
$C_{L_{\delta_E}}$	change in lift coefficient with elevator deflection angle, $\partial C_L/\partial\delta_E$, deg^{-1}
C_l	rolling-moment coefficient, $M_X/q_\infty Sb$

C_{l_p}	change in rolling-moment coefficient with roll rate, $\partial C_l/\partial(pb/2V)$, radian^{-1}
C_m	pitching-moment coefficient, $M_y/q_\infty Sc$
C_{m_q}	change in pitching-moment coefficient with pitch rate, $\partial C_m/\partial(qc/2V)$, radian^{-1}
C_{m_α}	change in pitching-moment coefficient with angle of attack, $\partial C_m/\partial\alpha$, deg^{-1}
$C_{m_{\dot\alpha}}$	change in pitching-moment coefficient with rate of change of angle of attack, $\partial C_m/\partial(\dot\alpha c/2V)$, radian^{-1}
$C_{m_{\delta_E}}$	change in pitching-moment coefficient with elevator deflection angle, $\partial C_m/\partial\delta_E$, deg^{-1}
c	reference chord, m
h	center-of-gravity location, x/c
h_m	maneuver point location, x/c
h_n	neutral point location, x/c
M_x	rolling moment, m-N
M_y	pitching moment, m-N
M	Mach number
n	load factor
p	roll rate, radians/sec
q	pitch rate, radians/sec
q_∞	dynamic pressure, N/m^2
S	projected wing area, m^2
V	airplane velocity, m/sec
x	longitudinal distance, m
α	angle of attack, deg
$\dot\alpha$	rate of change of angle of attack, radians/sec
δ_E	elevator deflection angle, deg
ζ	short-period damping ratio
ρ	air density, kg/m^3
ω	short-period damped natural frequency, radians/sec

Abbreviations

ALT	altitude
SST	supersonic transport
WT	airplane weight

CONFIGURATIONS, DATA, AND COMPUTATION

Two configurations representative of current transport aircraft designs were examined in this investigation. The general arrangement of the configurations is given in Fig. 1. The Boeing 707-320B airplane is generally familiar; the supersonic transport (SST) configuration is one of the early variable-sweep designs studied. Only the fully swept configuration is considered here.

Characteristic features of the Boeing 707-320B airplane pertinent to this investigation are its relatively high aspect ratio, 6.9, and its flexible structure. For planforms of this type, good results are normally expected of aerodynamic calculations.

The aspect ratio of the supersonic transport is low, 1.25, and severely tests the range of applicability of the aerodynamic analysis. Another feature of aerodynamic interest is the shear tie between the wing and the horizontal tail, which in the fully swept condition results in a discontinuity between the slopes of these surfaces at their juncture.

The experimental data for the 707 (see (4)) were obtained from flight tests of the full-scale elastic airplane and from wind-tunnel tests of an 0.035 scale rigid model. The Reynolds number of the wind-tunnel tests, based on the reference chord length (which for the full-scale airplane is 6.92 m), ranged from 1.8 to 3.0 million.

All experimental data for the SST (4) were derived from wind-tunnel tests. Two 0.015 scale models were used - one rigid and one elastic. The elastic model was constructed so that the deflections of the wing and tail surfaces under similar loading conditions duplicated as closely as possible those calculated for the proposed full-scale airplane at cruise conditions. Body flexibility was not duplicated; the body construction was the same as that ordinarily used for rigid models. Reynolds numbers of these tests were 15 to 21 million.*

Predicted values of aerodynamic quantities were in all cases obtained by use of aerodynamic influence coefficients. With the single exception of a portion of the dynamic stability calculations for the Boeing 707-320B airplane, these aerodynamic influence coefficients were computed by a method based on lifting surface theory (2,3). The 707-320B dynamic stability calculations deviating from this procedure employed aerodynamic influence coefficients obtained from lifting line theory. All calculations neglected the effects of wing thickness and, with one exception, those of body thickness as well.

Certain shortcomings inherent in the aerodynamic analysis, even in its complete form, should also be mentioned. Two in particular are important: (i) pressure distributions near the leading edge of the wing are not well represented, and (ii) pressures over each of the panels into which the planform is divided are presumed constant for that panel. For these and other reasons, the panel arrangement used in the calculations has decisively important effects on the accuracy of the results. Fig. 2 shows the paneling used for the computations of the present investigation; the paneling was arranged in accordance with the recommendations of (2).

Structural deflections, translational and angular, were calculated by use of structural influence coefficients. The coefficients employed for the 707-320B calculations were those used in the certification of the aircraft; they had, in addition, been verified by static load and vibration tests. For the SST conputations, experimental influence coefficients determined from directly measured deflections of the statically loaded wind-tunnel models were used.

To account for the airplane weight and inertia, part of the total mass was assigned to each panel to correspond to the airplane mass distribution over its planform. Each elemental mass was concentrated at the panel centroid. The effects of aerodynamic, inertial, and gravitational forces on the elastic deflections of the structure were then handled by two different methods. The first method, termed the "quasi-static-elastic," while including for each panel the inertial forces associated with airplane center of gravity acceleration, neglected the corresponding forces arising from panel accelerations relative to the airplane center of gravity. Panel deflections and the aerodynamic forces causing them were assumed to be exactly in phase at all times. This method is also known as the "static elastic" and "equivalent elastic" procedure. The second method, the "fully elastic" representation, recognized the effects of all inertial forces as well as gravitational forces, and used the concept of normal modes to represent the shape of the structure.

The term "rigid body" indicates a single, unique configuration. The shape of this configuration is that of the loaded quasi-static-elastic airplane with its mass properly distributed for the selected total weight in the cruise condition.

RESULTS AND DISCUSSION

The data summarizing the results obtained for the two configurations of this investigation are presented in Figs. 3 through 13. These figures have been arranged to illustrate first the accuracy of the analytical method as reflected by comparisons of static stability and control parameters (Figs. 3-8); second, the effects of elasticity on static longitudinal stability and control (Figs. 3-10); and, finally, the dynamic stability characteristics (Figs. 11-13).

The basic static derivatives considered are C_{L_α}, C_{m_α}, C_{l_p}, $C_{L_{\delta_E}}$, $C_{m_{\delta_E}}$, $d\delta_E/dV$, and $d\delta_E/dn$. Although Figs. 3 through 8 illustrate many of the effects of elasticity on the aerodynamic characteristics of the configurations, discussion of these effects is deferred to the section immediately following, where the additional data of Figs. 9 and 10 are introduced. All static stability calculations for the elastic airplane are based upon its quasi-static-elastic shape.

*Full-scale reference length was 48.2 m (158 ft).

Static Stability, Evaluation of Theory

Boeing 707-320B airplane.- To evaluate the accuracy of the theoretical calculations of lift and pitching moment, the values computed for lift curve slope, C_{L_α}, and for pitching-moment derivative, C_{m_α}, of the rigid airplane are compared in Fig. 3 with the experimental data obtained from wind-tunnel tests of a rigid model. Lift curve slope computations accounting for the effects of body thickness are also included in this figure. For C_{L_α}, the agreement of predicted with experimental values is considered good, the maximum discrepancy over the Mach number range for the thin body representation being of the order of 10 percent. Calculations of C_{L_α} using the thick-body representation provided even better comparison, the maximum discrepancy being reduced to less than 5 percent.

For C_{m_α}, the error in the magnitudes of the theoretical values is somewhat greater than it is for C_{L_α}, but here also the variation with Mach number is well represented.

As was previously explained, the aerodynamic calculations (except a portion of the 707-320B dynamic stability analysis) are based upon surface theory as contrasted with the lifting line theory frequently used for planforms of the type represented by this airplane. One reason for this choice stems from the results of comparative calculations with the two theories. In all cases the results obtained with lifting surface theory were in better agreement with experimental results than those derived from lifting line analysis.

In Fig. 4 values of C_{L_α} and C_{m_α} computed for the elastic airplane are compared with measurements made in flight at the altitudes and Mach numbers indicated. To provide a basis for evaluating these results, the rigid airplane characteristics of Fig. 3 are also shown. The agreement of the elastic body calculations with the flight data for C_{L_α}, and for C_{m_α} for the 108,900 kg airplane, is noticeably better than the agreement of the rigid body calculations with the same experimental data. Thus it may be concluded that the analytical method of (1) does account for the major effects of flexibility at these subsonic Mach numbers. The two experimental points for 129,500 kg gross weight, indicating that the stability of the 707-320B airplane increases with mass, should be interpreted cautiously. The scatter of the data for 108,900 kg shows that more evidence is required before any but qualitative conclusions can be drawn. It should further be noticed that the difference between calculated and flight values for 108,900 kg gross weight approximates -0.003 and that this difference is about the same as that shown in the C_{m_α} comparison of Fig. 3.

The variation with Mach number of C_{l_p}, change in rolling-moment coefficient with rate of roll, is shown in Fig. 5. Here also the agreement of calculated with measured results is reasonably good. This conclusion is also supported by the data of Fig. 6, in which the variation of elevator angle with velocity $d\delta_E/dV$ and with load factor $d\delta_E/dn$ have been plotted. The good agreement observed in this latter figure is of more than passing significance, in that it provides an appraisal of the overall validity of the analysis. The experimental values are measured directly and with reasonable accuracy; the predicted values are determined indirectly, from calculated values of such basic derivatives as C_{L_α}, C_{m_α}, C_{m_q}, $C_{m_{\delta_E}}$, etc.

Supersonic transport.- Comparisons of predicted and experimental values of the angle-of-attack derivatives C_{L_α} and C_{m_α} for the SST configuration at Mach numbers of 1.6 and 2.7 are presented in Fig. 7. These data are plotted as functions of free-stream dynamic pressure for both rigid and elastic models. For the elastic wind-tunnel model the effects of model mass, and of mass distribution, were calculated and found to be negligible.

Predicted values of C_{L_α} for both the rigid and flexible models, when compared to the experimental data, show good agreement. The discrepancies that do occur are less than 4 percent of the experimental values.

Analytical calculations of C_{m_α} for the rigid model do not agree with the experimental values measured in the wind-tunnel tests. This result is not peculiar to this configuration nor to the thin body assumption. Experience with the aerodynamic analysis using thick body representation, while not yet extensive, indicates that the disagreement observed here both in size and direction (underestimation of the static stability) is usually encountered. The error appears to be inherent in the aerodynamic analysis as it is presently formulated. Among the possible causes may be the failure to accurately account for leading edge pressure representation and the fact that chordwise pressure distributions near the wing tip, as shown in (2) and (3), are noticeably inaccurate. These and other possibilities are currently being investigated at the NASA, Ames Research Center by wind-tunnel tests of pressure distributions models.

It should also be noted that the experimental measurements of C_{m_α} at lift coefficients of 0.02 and 0.08 shown in Fig. 7 disagree with one another. This disagreement shows that C_{m_α} is not independent of C_L; consequently, C_m varies nonlinearly with angle of attack. The formulation of the aerodynamic theory, depending as it does upon linear approximations, obviously cannot account for this nonlinear effect.

Comparisons of the predicted elevator control surface derivatives $C_{L_{\delta_E}}$ and $C_{m_{\delta_E}}$ for the SST configuration are illustrated in Fig. 8. For $C_{L_{\delta_E}}$ both rigid and elastic calculated values

generally agree well with the experimental values, except for the rigid model at 1.6 Mach number. The agreement is also good for the rigid body values of $C_{m_{\delta_E}}$. Here, however, because the elastic and experimental values disagree seriously and because calculated values of C_{m_α} are, as discussed previously, unreliable, values predicted for $C_{m_{\delta_E}}$ should be viewed with caution. It should also be observed that the predictions are unconservative.

Static Stability, Effects of Elasticity

The data used to appraise the effects of elasticity on the static stability and control of the Boeing 707-320B airplane are contained in Figs. 4-6, and in Fig. 9. For the supersonic transport configuration the relevant information appears in Figs. 7, 8, and 10. All pitching-moment data are, for the 707-320B, referred to the 25-percent chord point; and for the SST, to the 64-percent chord point.

Boeing 707-320B airplane.- The effects of elasticity on the stability derivatives C_{L_α} and C_{m_α} may be inferred by comparing the curves of Fig. 4 calculated for the rigid and elastic body shapes. For both derivatives it is clear that the changes are large and unfavorable, and that these differences increase sharply at Mach numbers above 0.4. For example, at 0.6 Mach number and 3050 m altitude the loss in C_{L_α} is 20 percent of the rigid body value, and in C_{m_α}, 50 percent. The rolling moment derivative C_{l_p} also is noticeably affected (Fig. 5). For these same conditions the reduction here also approximates 50 percent.

It is interesting to examine the trend with Mach number of the magnitudes of the differences between rigid and elastic values calculated for C_{L_α}, C_{m_α}, and C_{l_p}. As an example, at 0.2 Mach number the difference in the C_{L_α} curves is approximately 0.0025; at 0.4, 0.009; and at 0.8, 0.037. The loss experienced in C_{L_α} thus varies more or less quadratically with Mach number. This same result is also found for C_{m_α} and for C_{l_p}. Since the dynamic pressure at constant altitude likewise varies as the square of the Mach number, the data indicate that for this airplane losses due to elasticity, at constant altitude, are primarily associated with changes in dynamic pressure.

Flight test data for C_{m_α} in Fig. 4 indicate that the effects of elasticity also change with changes in the airplane mass. The reduction in stability appears to be greater for the lighter weight airplane.

The differences between the rigid and elastic values of $d\delta_E/dn$, and of $d\delta_E/dV$ at Mach numbers below 0.3, illustrated in Fig. 6, are negligible. This result is attributed to the fact that, while changes in the basic derivatives are material, the changes neutralize each other in the process of combining these derivatives to calculate $d\delta_E/dn$ and $d\delta_E/dV$. Accordingly, the elastic effects observed here are considered to be a peculiarity of the 707-320B airplane; they may or may not be encountered in other designs. Above 0.3 Mach number the differences in $d\delta_E/dV$ increase noticeably, and in the direction of increased stability.

The effects of elasticity on the longitudinal stability of the 707 airplane are further illustrated in Fig. 9 by the comparison of calculated values of static margin and maneuver point for both rigid and elastic airplanes. The loss in stability is seen to be significant for all flight conditions. For flight near Mach number 0.6 the incremental change in static margin is 4 percent of the reference chord, amounting to approximately 20 percent of the total center-of-gravity range for this airplane. (Center-of-gravity range for the 707 is 19 percent of the reference chord.) Changes in maneuver point for the rigid and elastic airplane are approximately the same as the change that occurred in static margin.

Supersonic transport.- The effects of elasticity on the lift and pitching-moment coefficients of the SST configuration are shown in Fig. 7 for Mach numbers 1.6 and 2.7. A comparison of C_{L_α} measured for the rigid and elastic models shows that significant losses occur at both Mach numbers throughout the range of dynamic pressures investigated. The relative magnitude of these losses is approximately the same at both Mach numbers (15 percent at 1.6 and 12 percent at 2.7 Mach number). The deterioration of pitching-moment coefficient, as measured by C_{m_α}, is even more pronounced. Losses as great as 50 percent were found experimentally. These losses also persist throughout the range of dynamic pressures for both Mach numbers.

The effects of elasticity on the control derivatives $C_{L_{\delta_E}}$ and $C_{m_{\delta_E}}$ (Fig. 8) follow the same pattern. The losses are large (50 percent roughly of rigid body values) at all Mach numbers. These effects are indicated both by the experimental observations and by the theoretical predictions.

A further appreciation of the effects of elasticity on the longitudinal stability characteristics of this configuration may be obtained from examination of the shift in neutral point location. Fig. 10 presents this parameter plotted as a function of dynamic pressure for 2.7 Mach number. The variations of gross weights and dynamic pressures in Fig. 10 encompass the design operating range. Thus, 142,500 kg is the weight of the basic aircraft without fuel or payload, and 302,800 kg is the weight fully loaded with maximum fuel and payload. For the 835 m^2 (9,000 ft^2) reference wing area of this airplane the lift coefficients range from 0.073 to 0.156 at the lowest dynamic pressure, and from 0.027 to 0.057, at the highest (design cruise C_L is 0.09 to 0.12). Although, as noted in the

figure, the center of gravity (and also the moment reference point) was fixed at 64 percent of the reference chord for these calculations, the mass distribution was not constant; it was changed in each case to reflect the actual distribution expected in flight for the fuel and payload assumed.

The final design provided for a variation in the center-of-gravity location of 5 percent (0.05 reference chord). Fig. 10 shows that at 2.7 Mach number the neutral point shifts from 0.01 reference chord forward to 0.02 aft, that is, 0.03 reference chord or 60 percent of the center-of-gravity requirement itself. This shift results from changes both in dynamic pressure and in airplane load (gross weight and mass distribution), the effect of this latter quantity being greatest when the gross weight is smallest.

It is evident, of course, that at 2.7 Mach number the curves corresponding to maximum fuel and payload, and to empty weight are not realistic boundary conditions and that 0.03 total shift in neutral point would never be met in practice. It is important to remember, however, that the range of dynamic pressures considered in this figure can be encountered at Mach numbers as low as 1.0 (1100 m or 3620 ft altitude). The variation in gross weight and mass distribution for which dynamic pressures as high as 62,200 N/m^2 (1300 lb/ft^2) must be reckoned with is therefore somewhat greater than Fig. 10 implies. Whether or not the neutral point remains within the envelope of Fig. 10 throughout the Mach number range depends, among other things, on the magnitudes of the differences between C_{m_α} for the rigid airplane and C_{m_α} for the elastic airplane.

In any event, the conclusion is inescapable that this effect of elasticity confronts the designer with a major problem. To make certain that adequate longitudinal stability exists for all center-of-gravity locations and flight conditions, the elastic effects must be completely analyzed at the very beginning of the airplane design. The calculations summarized in Fig. 10 illustrate that the method presented in this paper provides the means required in early evaluations.

Dynamic Stability

While use of the quasi-static-elastic representation of the aircraft structure to analyze steady state flight characteristics is inherently a technically sound approach, the same remark cannot in general be made for dynamic stability, although this is the representation commonly used. The lower structural frequencies and the short-period frequency of the aircraft motion may be close enough to result in interchange of significant amounts of energy. To examine this possibility, and to determine the magnitude of the effects for the subject configurations, calculations were made and the results summarized in Figs. 11, 12, and 13. In the calculations the structural shape was represented (as described in (1)) by its normal modes, the number used varying from 0 (rigid body) to 20 for the SST and to 14 for the Boeing 707.

Supersonic transport.- Fig. 11 indicates that for the SST model neither damping ratio nor frequency is materially affected by elasticity at any of the three Mach numbers investigated. The fact that the damping ratios computed both from quasi-static-elastic and the fully elastic analyses (20 normal modes) are always smaller than those derived from rigid body analysis is, however, an indication that damping deteriorates with elasticity. No significance is attached to the uniformly smaller damping ratios computed using the quasi-static-elastic representation as compared to the results for 20 normal modes.

Fig. 12 shows the effects on damping ratio and frequency of varying the number of normal modes used in the fully elastic analysis. (Values shown for 0 modes in this figure differ from the rigid body values of Fig. 11 because $C_{m_{\dot\alpha}}$ and $C_{L_{\dot\alpha}}$ were not included in the normal mode calculations.) It is apparent for all three Mach numbers that the number of normal modes used had virtually no effect on either damping ratio or frequency - a result entirely consistent with the data of Fig. 11. Some clue to the reasons for this result is furnished by a comparison of structural frequencies with the frequency of motion. Values of the former quantity are 1.6 Hz for the primary mode, 2.33 Hz for the secondary, and 3.88 for the tertiary. The corresponding ratios to frequency of motion (using the value 2.8 Hz) at 2.7 Mach number are 5.7, 8.3, and 12.1. Structural and motion frequencies are therefore fairly far removed from one another, and this separation together with the damping forces present apparently nullifies any effects of coupling.

Boeing 707-320B airplane.- Consideration of similar data for the Boeing 707 airplane (Fig. 13) provides further support for this hypothesis. The first three structural fequencies of this configuration are 1.24 Hz, 2.92 Hz, and 3.39 Hz (ratios to rigid body motion: 3.5, 8.3, and 9.7). The lowest structural frequency is therefore somewhat closer to the frequency of motion than it is for the SST, and it is seen that the computed value of damped frequency for the elastic case does differ detectably from the rigid body value. The damping ratio, however, is virtually unaffected. The inference of these results, applied to other airplanes, is that further reduction in the ratio of primary structural frequency to the rigid body motion frequency below 3.5 would induce coupling between structural and rigid body motions.

In summary, while some elastic effects on the dynamic motion of both of these aircraft are apparent, the effects are nowhere large, and quasi-static-elastic or even a rigid body analysis is sufficiently accurate for most design purposes. Other designs, particularly those for which the primary structural frequencies are less than four times the frequency of rigid body motion, should be quite carefully investigated using a completely elastic representation.

CONCLUDING REMARKS

An examination of the principal longitudinal stability and control derivatives of two representative flexible airplane configurations, determined both analytically and experimentally, indicated that:

1. Except for the pitching-moment derivatives, the analytical procedure provided useful values of the principal static stability, control, and dynamic stability derivatives.

2. Discrepancies for the most part are probably attributable to errors inherent in the aerodynamic theory.

3. The fully dynamic representation of the structure based on normal mode theory would not be required for either of these two configurations. A simplified structural arrangement ("quasi-static-elastic") provided results of substantially the same accuracy.

4. The static stability characteristics of both configurations were affected strongly by elasticity and, in most cases, adversely.

5. The longitudinal control derivatives examined were also significantly and unfavorably affected.

6. Dynamic stability characteristics, as measured by damping ratio and damped frequency, were not greatly affected by elasticity. For both aircraft, however, structural frequencies were relatively far from the frequency of rigid body motion, and the data indicate that without this separation major effects might be encountered.

REFERENCES

1. Dusto, A. R.: An Analytical Method for Predicting the Stability and Control Characteristics of Large Elastic Airplanes at Subsonic and Supersonic Speeds, Part I - Analysis. Paper presented at the AGARD Flight Mechanics Panel Meeting on Aeroelastic Effects From a Flight Mechanics Standpoint, Marseille, France, April 1969.

2. Woodward, F. A.; Tinoco, E. N.; and Larsen, J. W.: Analysis and Design of Supersonic Wing-Body Combinations, Including Flow Properties in the Near Field - Part I - Theory and Application. NASA CR 73106, 1967.

3. Woodward, F. A.: Analysis and Design of Wing-Body Combinations at Subsonic and Supersonic Speeds. Journal of Aircraft, vol. 5, no. 6, Nov.-Dec. 1968.

4. Members of the Aerodynamics and Structures Research Organizations, The Boeing Company, Commercial Airplane Division, Renton, Washington: An Analysis of Methods for Predicting the Stability Characteristics of an Elastic Airplane. NASA CR 73277, 1968.

FIGURE TITLES

Fig. 1.- Aircraft general arrangement.

Fig. 2.- Airplane paneling.

Fig. 3.- Calculated and experimental angle-of-attack derivatives, rigid body, Boeing 707-320B.

Fig. 4.- Calculated and experimental angle-of-attack derivatives, elastic body, Boeing 707-320B.

Fig. 5.- Calculated and experimental roll-rate derivative, elastic body, Boeing 707-320B.

Fig. 6.- Calculated and experimental velocity and load-factor derivatives, elastic body, Boeing 707-320B.

Fig. 7.- Calculated and experimental angle-of-attack derivatives, rigid body and elastic body, supersonic transport.

Fig. 8.- Calculated and experimental elevator deflection angle derivatives, rigid body and elastic body, supersonic transport.

Fig. 9.- Effects of elasticity on static margin and maneuver point, Boeing 707-320B.

Fig. 10.- Effect of elasticity on neutral point location, supersonic transport.

Fig. 11.- Effect of elasticity on short-period damping and frequency, supersonic transport.

Fig. 12.- Effect of number of normal modes on short-period damping and frequency, supersonic transport.

Fig. 13.- Effect of number of normal modes on short-period damping and frequency, Boeing 707-320B.

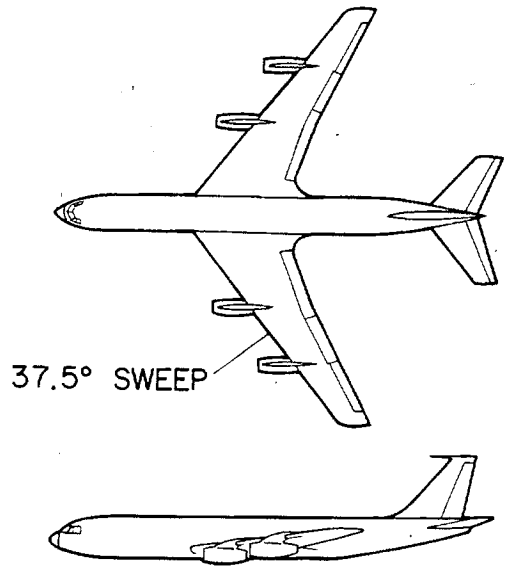

(a) BOEING 707 - 320B

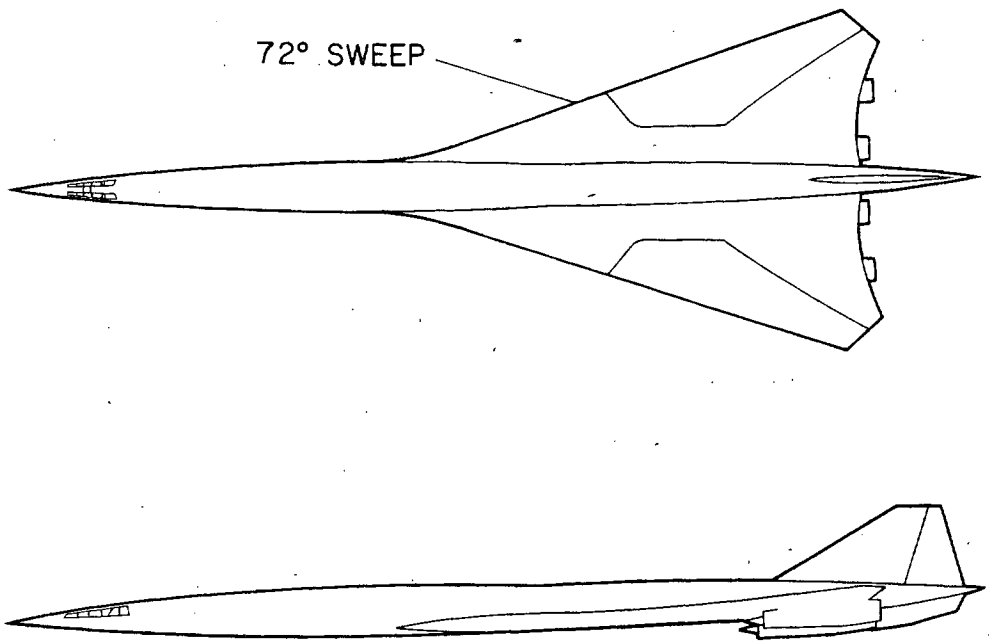

(b) REPRESENTATIVE SUPERSONIC TRANSPORT (SST)

Figure 1.- Aircraft general arrangement.

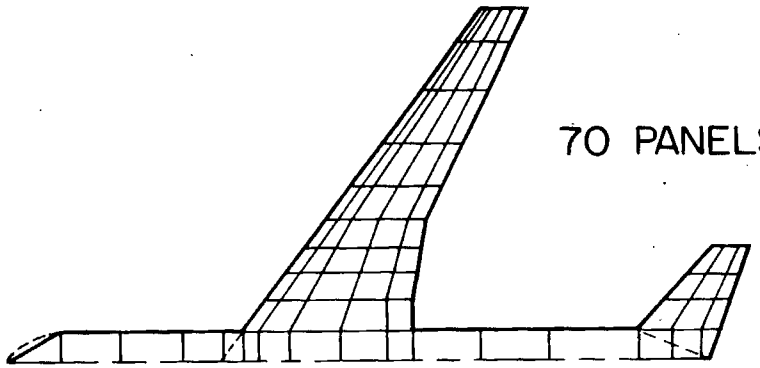

a) BOEING 707 - 320B

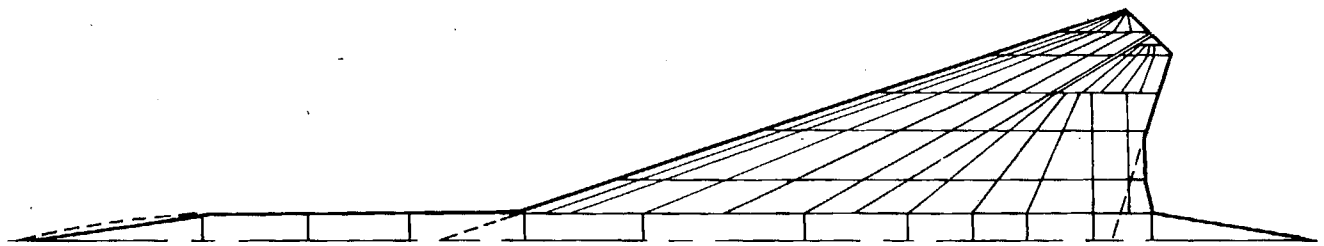

b) REPRESENTATIVE SUPERSONIC TRANSPORT (SST)

Figure 2.- Airplane paneling.

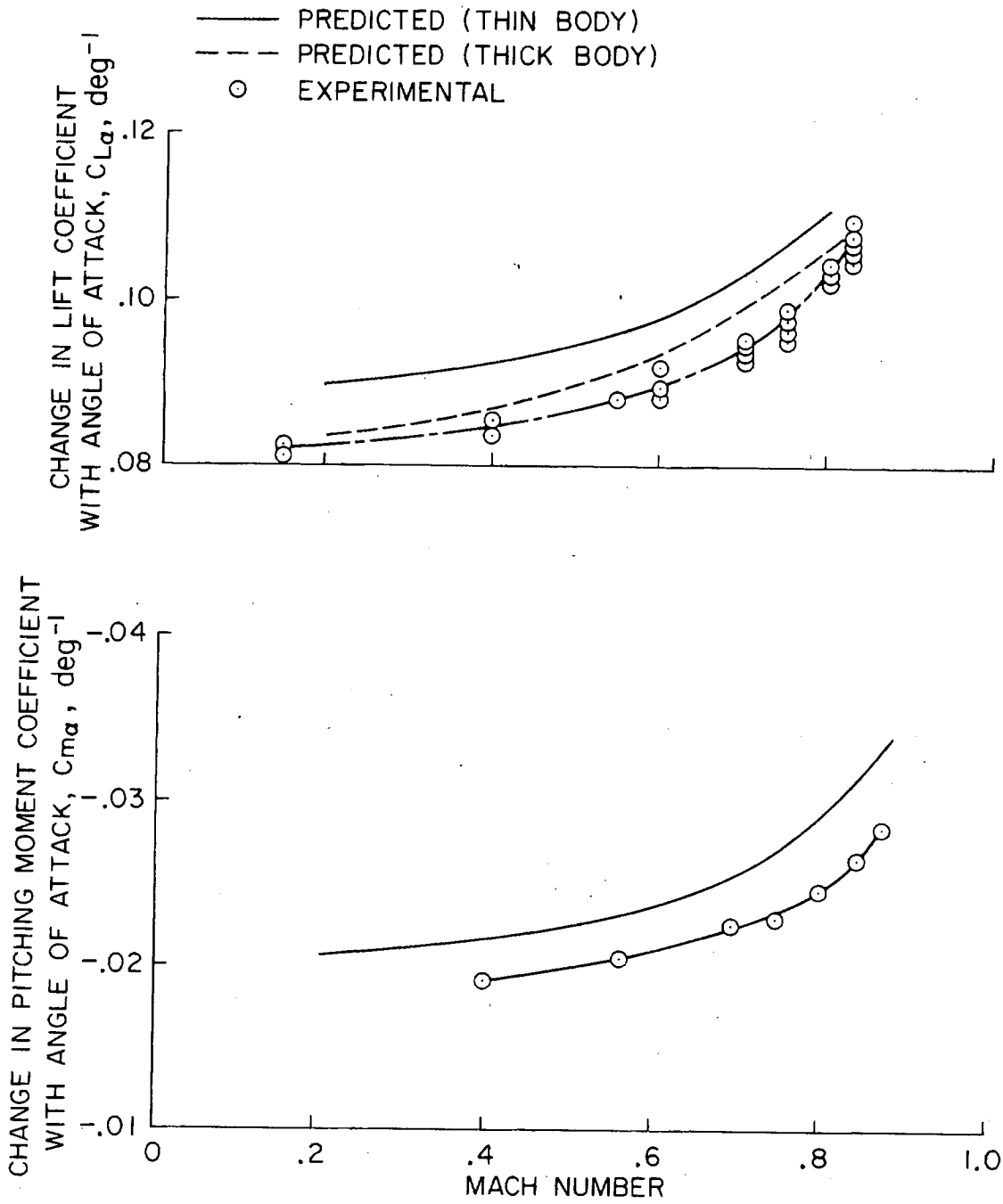

Figure 3.- Calculated and experimental angle-of-attack derivatives, rigid body, Boeing 707-320B.

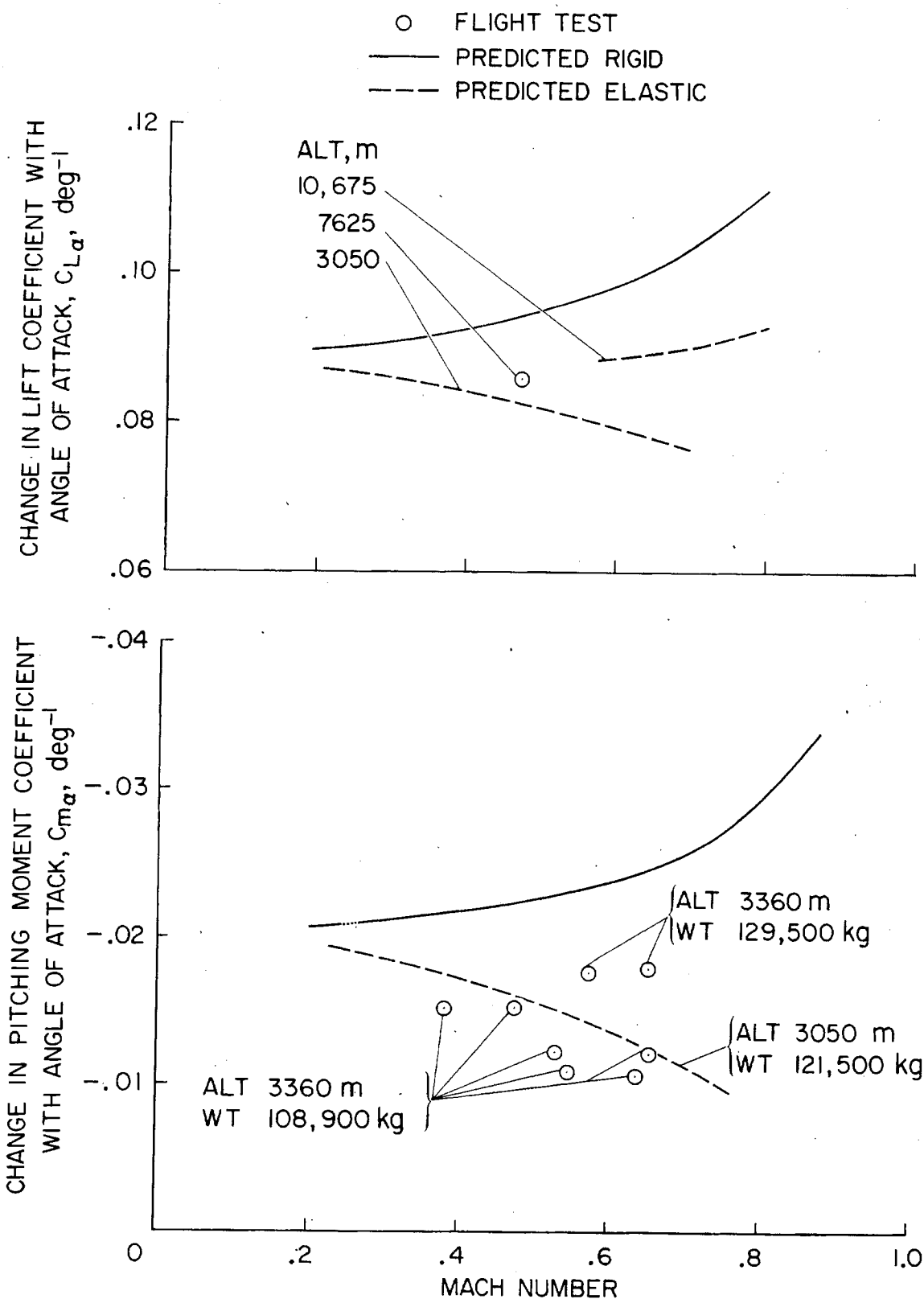

Figure 4.- Calculated and experimental angle-of-attack derivatives, elastic body, Boeing 707-320B.

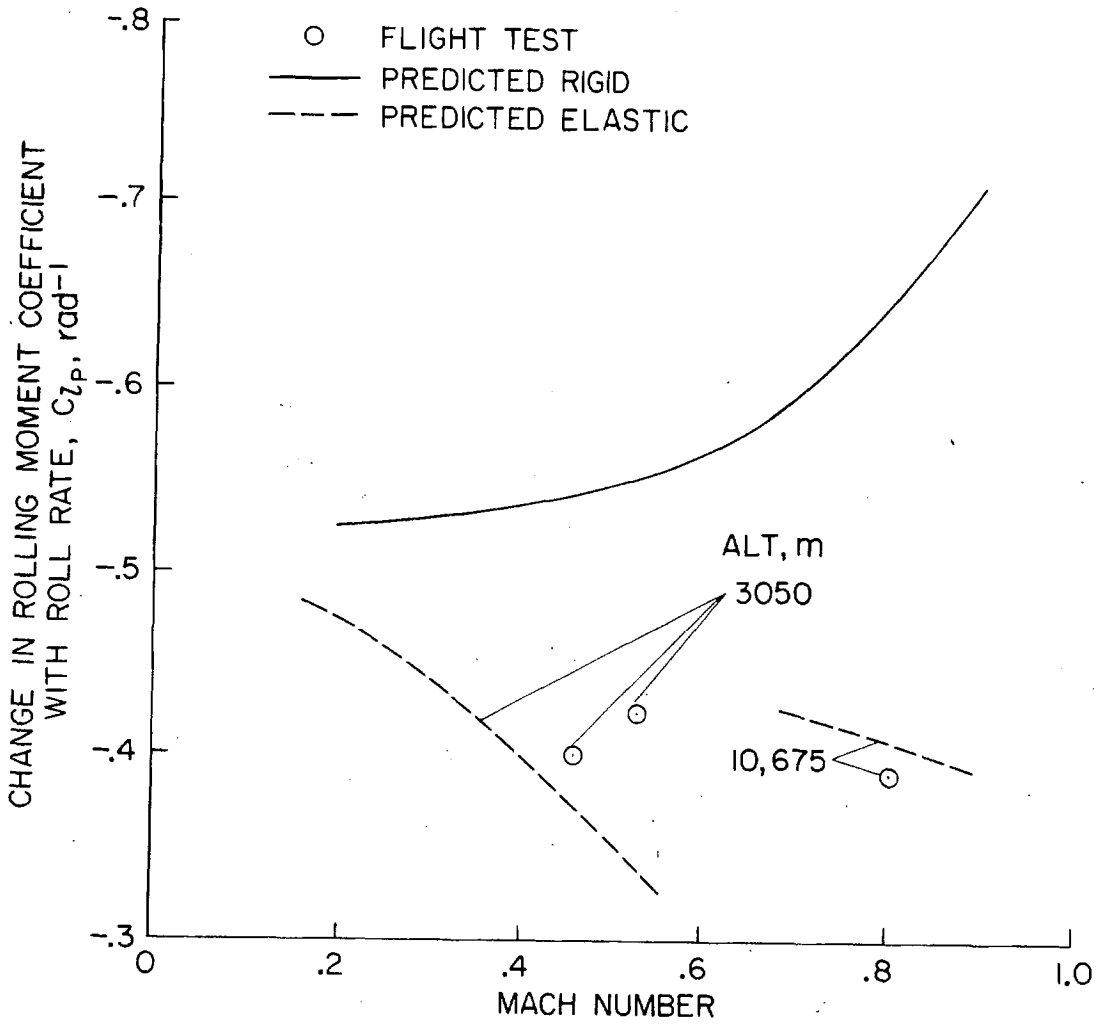

Figure 5.- Calculated and experimental roll rate derivative, elastic body, Boeing 707-320B.

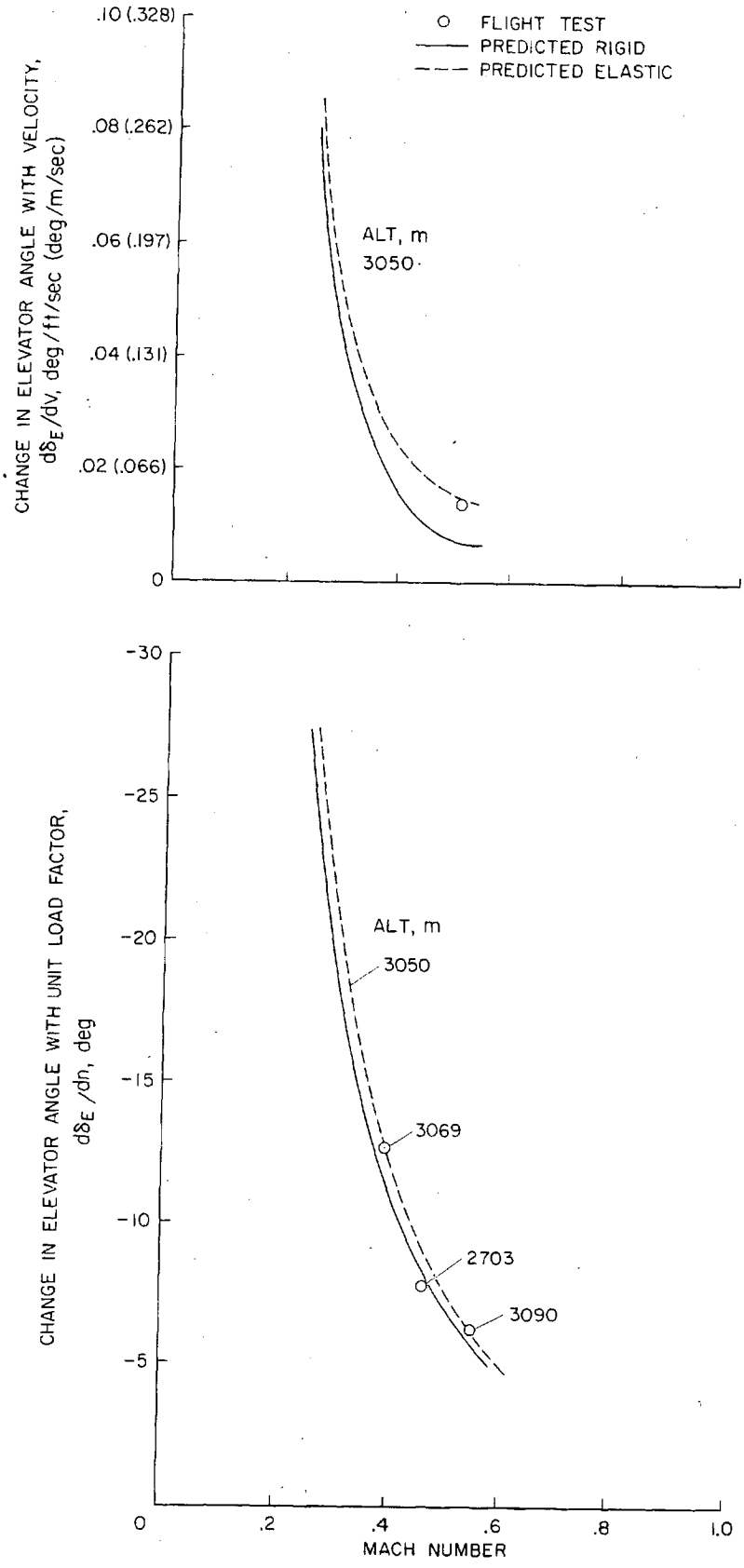

Figure 6.- Calculated and experimental velocity and load factor derivatives, elastic body, Boeing 707-320B.

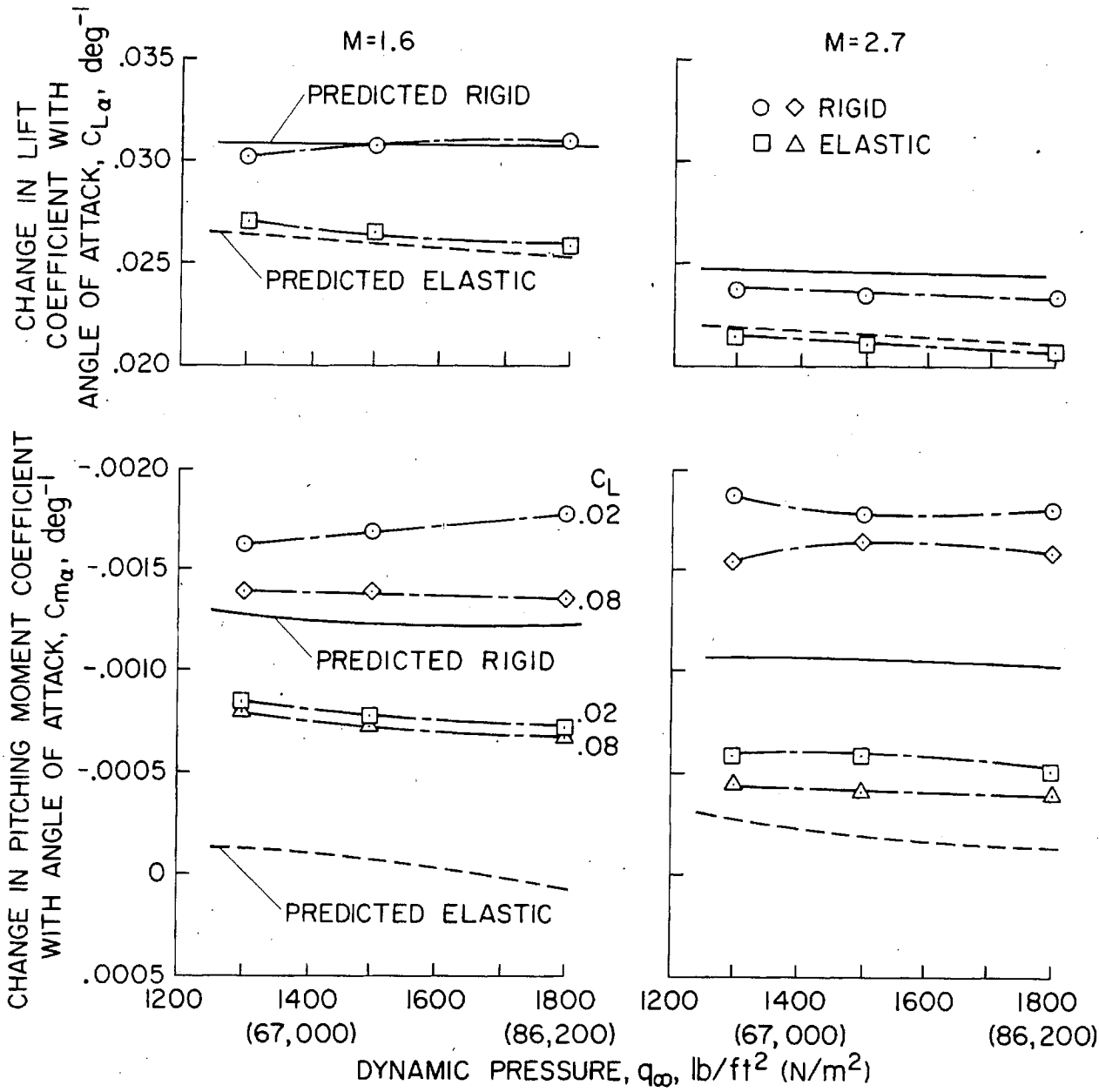

Figure 7.- Calculated and experimental angle-of-attack derivatives, rigid body and elastic body, supersonic transport.

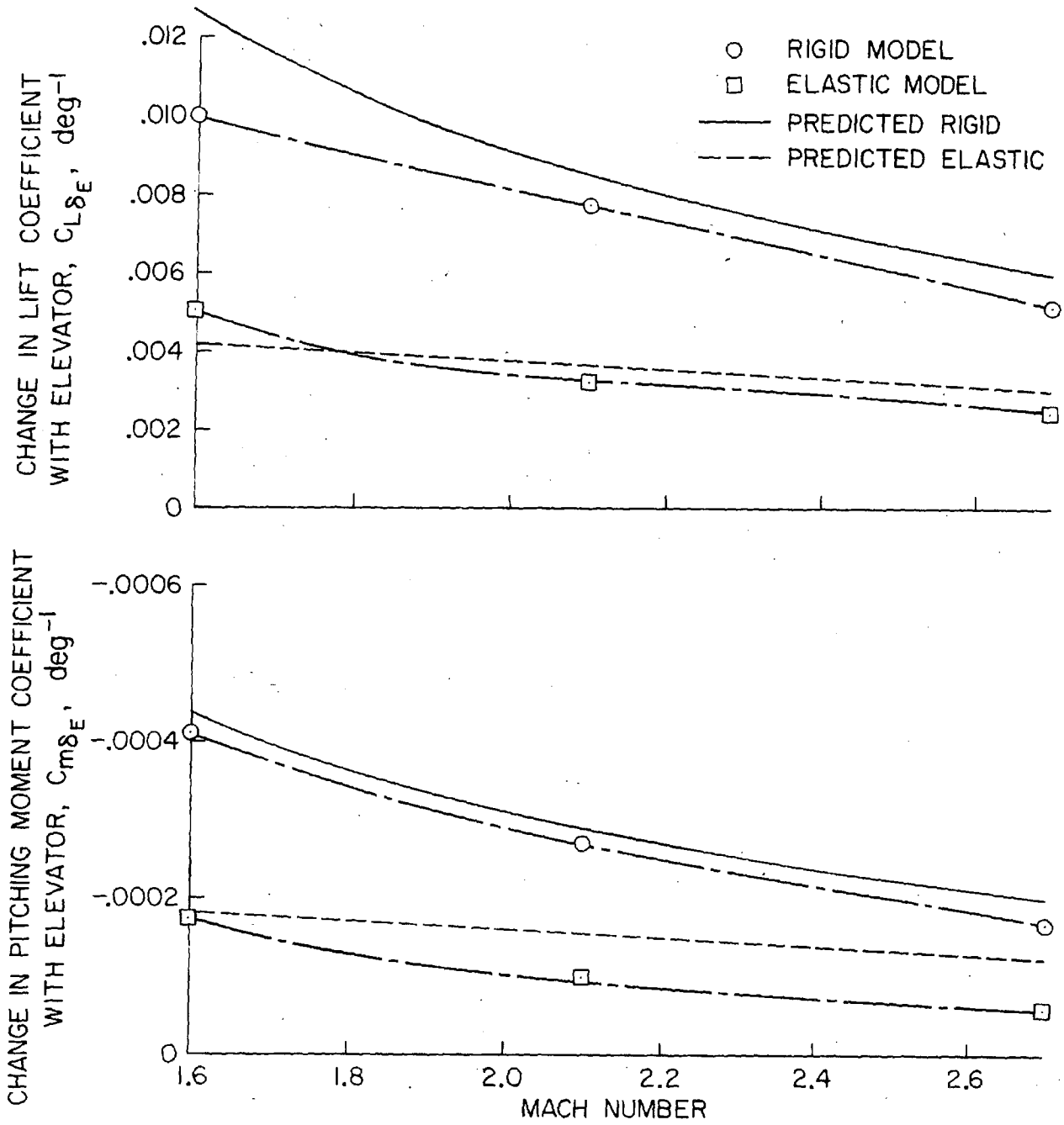

Figure 8.- Calculated and experimental elevator deflection angle derivatives, rigid body and elastic body, supersonic transport.

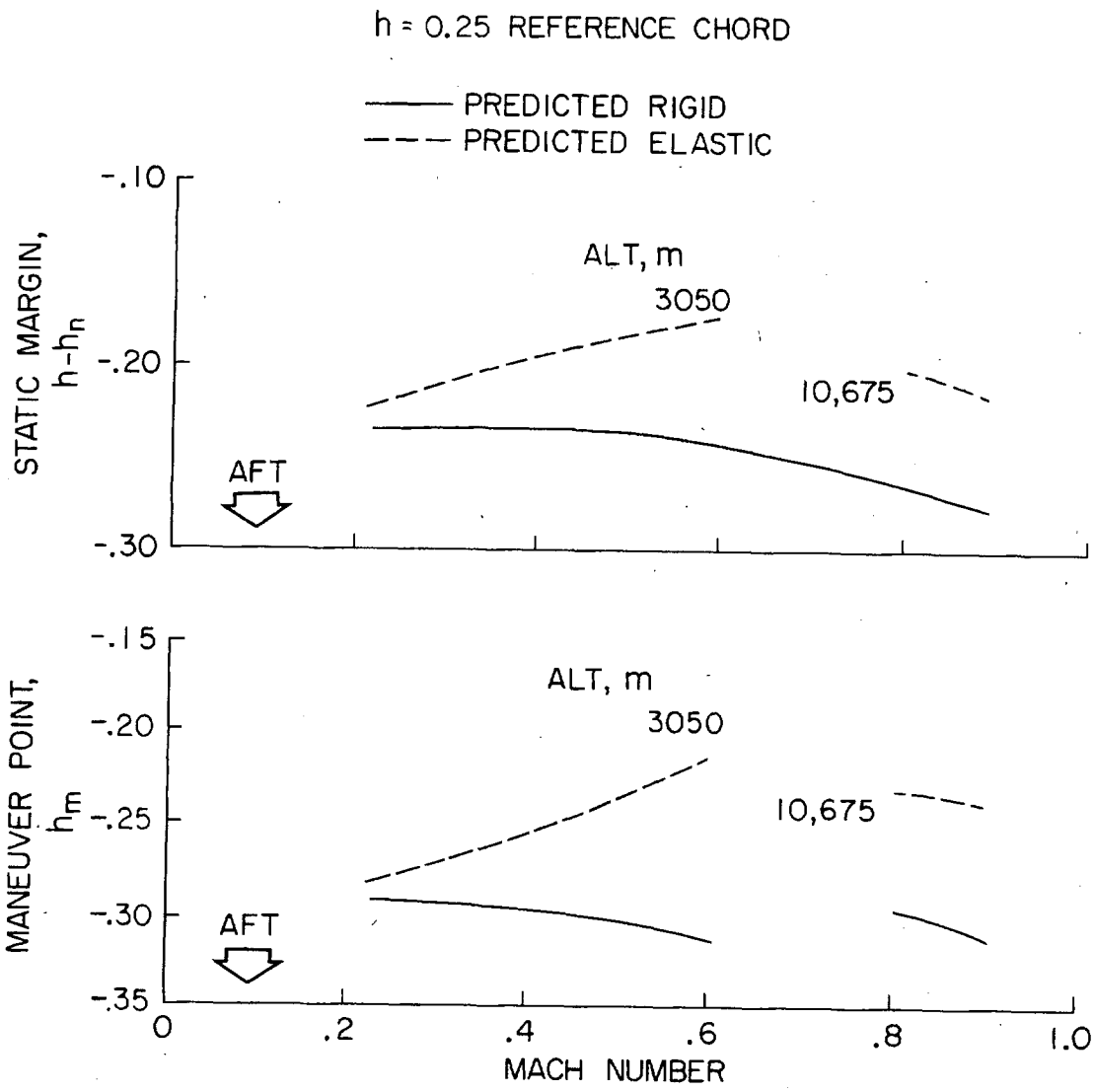

Figure 9.- Effects of elasticity on static margin and maneuver point, Boeing 707-320B.

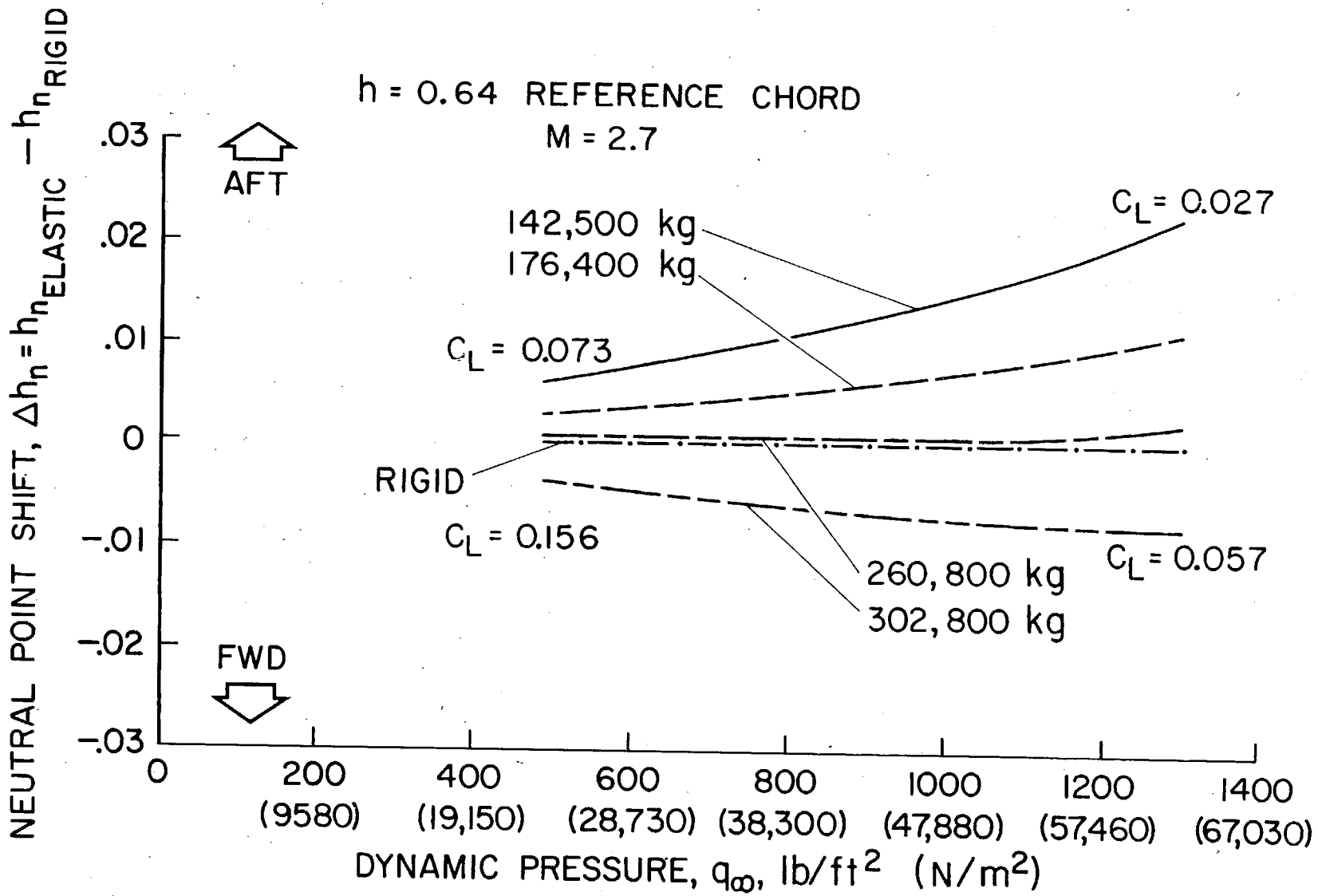

Figure 10.- Effect of elasticity on neutral point location, supersonic transport.

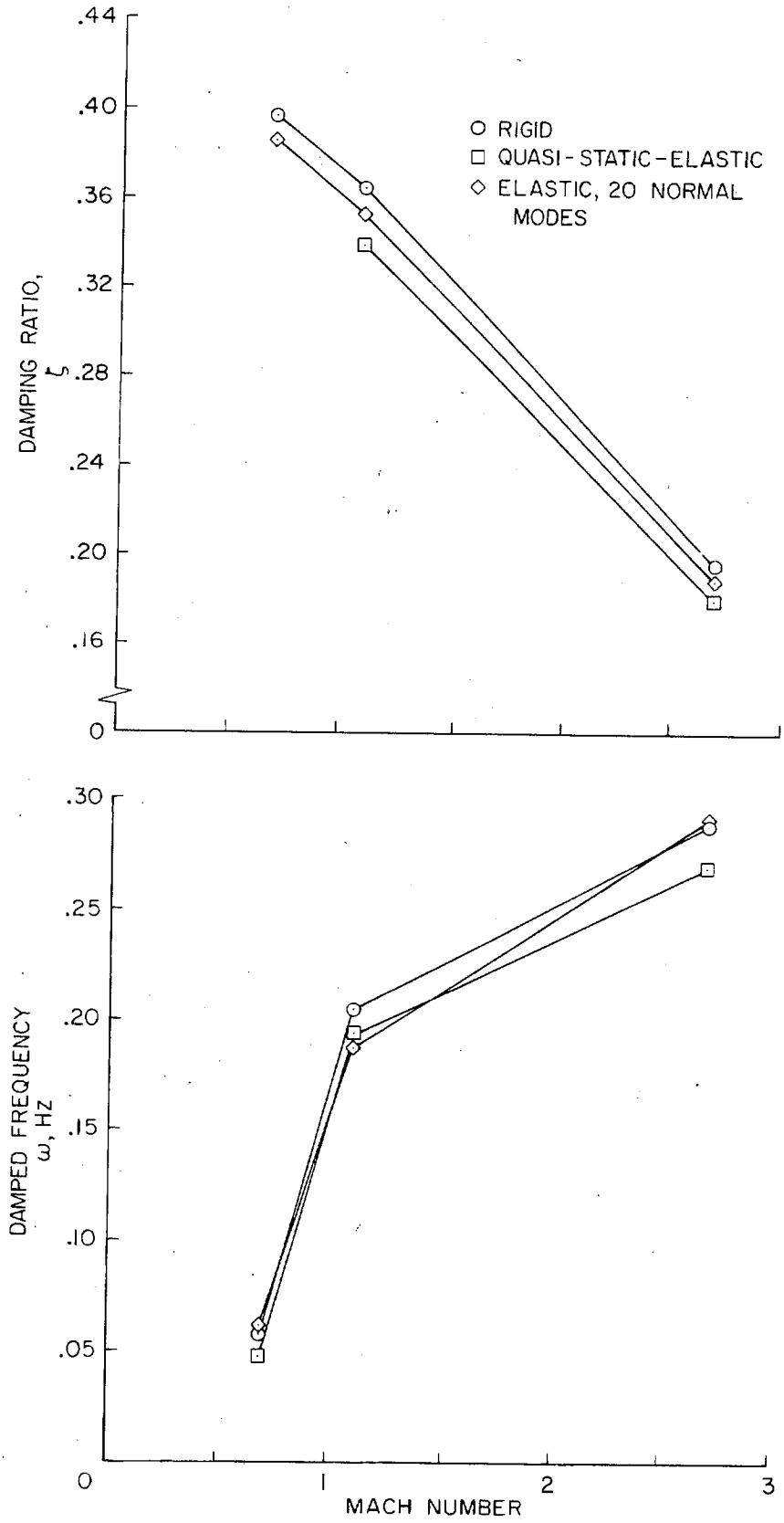

Figure 11.- Effect of elasticity on short period damping and frequency, supersonic transport.

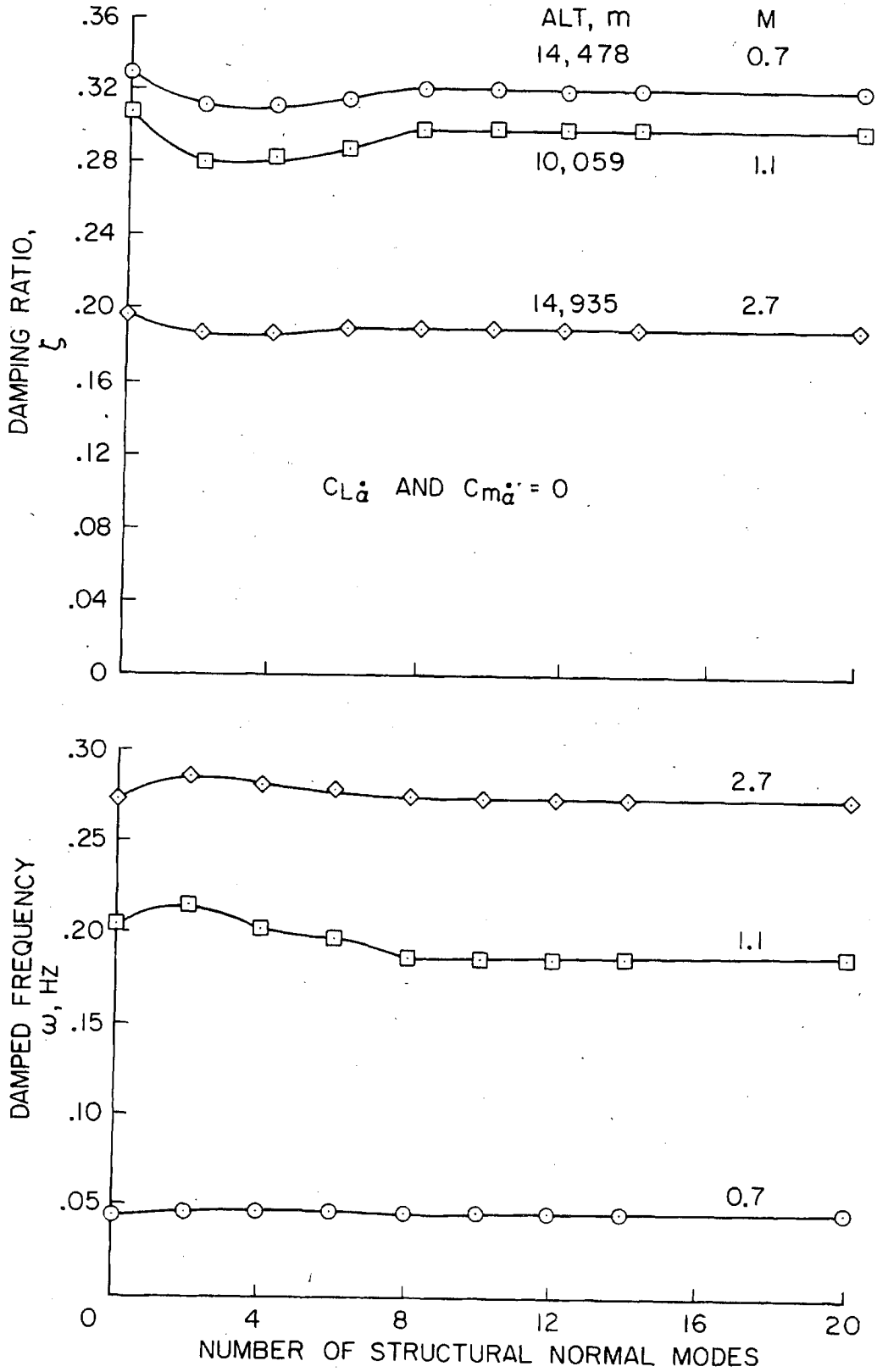

Figure 12.- Effect of number of normal modes on short period damping and frequency, supersonic transport.

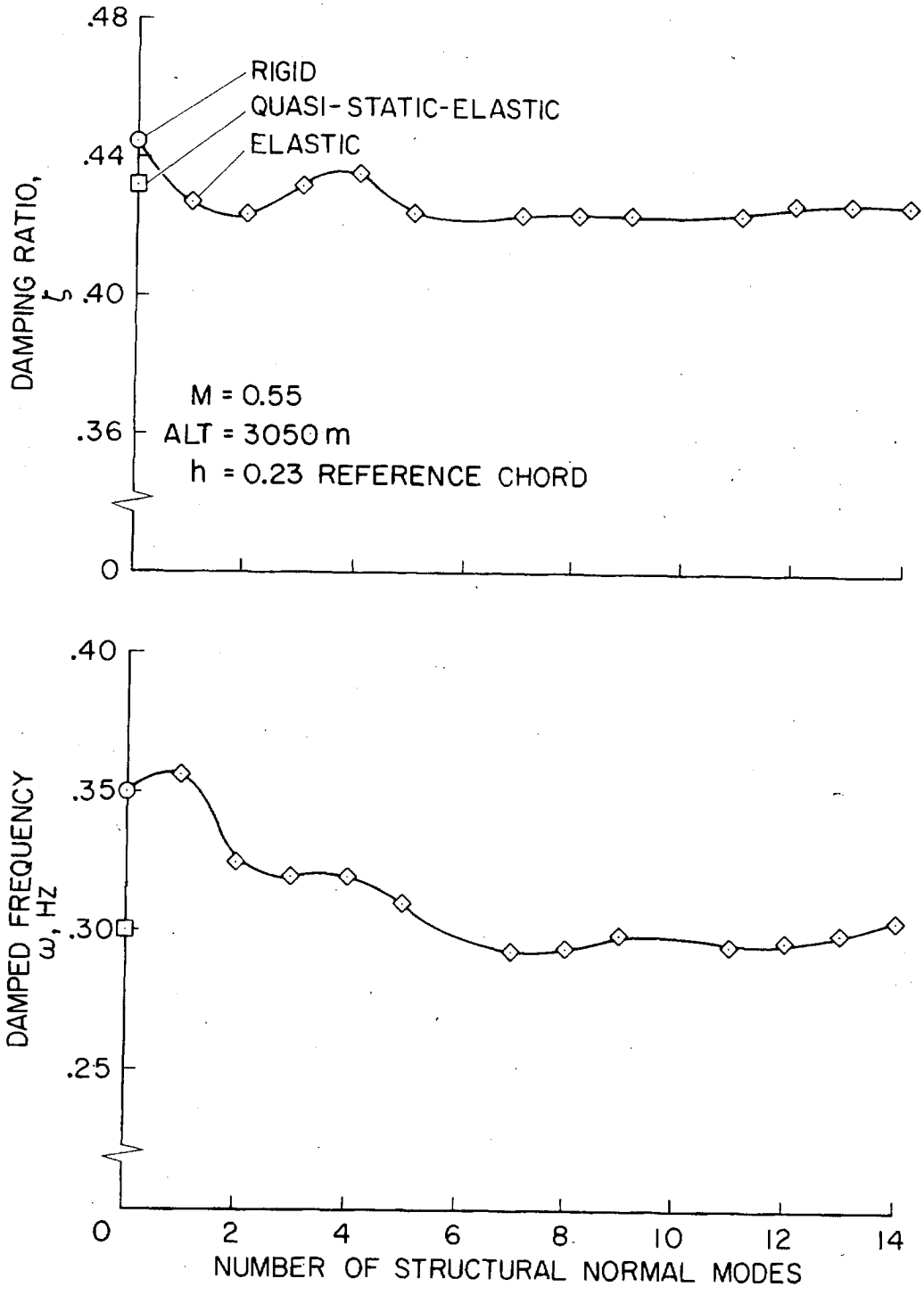

Figure 13.- Effect of number of normal modes on short period damping and frequency, Boeing 707-320B.